JOURNAL OF SYNCHROTRON RADIATION

ISSN 1600-5775

Counting-loss correction method based on dual-exponential impulse shaping

Yi Liu, Ming Wang,* Wenjie Wan, Jianbin Zhou, Xu Hong, Fei Liu and Jie Yu

College of Nuclear Technology and Automation Engineering, Chengdu University of Technology, Chengdu 610059, People's Republic of China. *Correspondence e-mail: wangmingming13@qq.com

Received 14 March 2020
Accepted 9 August 2020

Edited by Y. Amemiya, University of Tokyo, Japan

Keywords: counting loss correction; dual-exponential signal; unit-impulse-response; dead-time.

Under the condition of high counting rate, the phenomenon of nuclear pulse signal pile-up using a single exponential impulse shaping method is still very serious, and leads to a severe loss in counting rate. A real nuclear pulse signal can be expressed as a dual-exponential decay function with a certain rising edge. This paper proposes a new dual-exponential impulse shaping method and shows its deployment in hardware to test its performance. The signal of a high-performance silicon drift detector under high counting rate in an X-ray fluorescence spectrometer is obtained. The result of the experiment shows that the new method can effectively shorten the dead-time caused by nuclear signal pile-up and correct the counting rate.

1. Introduction

Owing to the dead-time of a measurement system, the relationship between the incidence rate and counting rate is nonlinear under the condition of high radiation levels. The dead-time correction method or the fast and slow dual-channel measurement method (Hong *et al.*, 2018) are used to correct the analysis system in energy spectrum analysis. The dead-time caused by nuclear signal pile-up is the main reason affecting the counting rate accuracy. Pulse shaping methods (Cano-Ott *et al.*, 1999; Bolić & Drndarević, 2002; Ehrenberg *et al.*, 1978; Imperiale & Imperiale, 2001; Jordanov, 2016; Jordanov & Knoll, 1994) can be used to correct the counting rate. For the fast channel method, Huang *et al.* (2017) studied the single-exponential nuclear signal pile-up discrimination system, and Hong *et al.* (2018) studied the deconvolution unit impulse shaping system – these two systems aimed at solving the problem of pile-up dead-time. However, the dead-time correction of the single exponential fast shaping method is still barely satisfactory and therefore its practicality is limited.

This paper analyzes the dual-exponential characteristic of the nuclear signal, and then the transfer function between dual-exponential signal and impulse response is derived. The fast-shaping method of the impulse response based on dual-exponential signals can effectively reduce the dead-time and improve the counting rate accuracy of the measurement system.

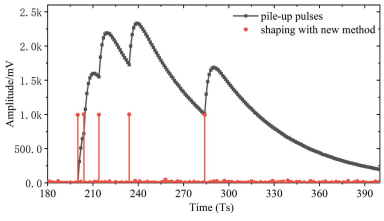

2. Theory

2.1. Dual-exponential impulse shaping theory

In the digital processing of pulses, pulse discrimination systems are used to discriminate the pulses' generation time and count the pulses. As shown in Fig. 1, the input of the transfer function model of the system is an ideal dual-expo-

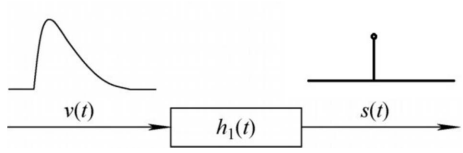

Figure 1
Pulse discrimination system model.

nential pulse (Sun *et al.*, 2017) and of which the output is an ideal impulse response function. The time when the impulse response emerges can be used to locate the generation time of the pulse, and the number of impulse responses can be used to correct the counting rate.

In the system, the input dual-exponential pulse can be expressed as

$$v_i(t) = A[\exp(-t/M) - \exp(-t/m)], \qquad t \geq 0, \tag{1}$$

where M and m represent the decay time constants of the slow and fast components, respectively. The impulse response of the system is given as

$$v_o(t) = A\delta(t), \qquad t \geq 0. \tag{2}$$

By using a Z transformation for equations (1) and (2), the transform function of the shaping system is given by

$$H(z) = \frac{V_o[z]}{V_i[z]} = \frac{\left(1 - d_1 z^{-1}\right)\left(1 - d_2 z^{-1}\right)}{(d_1 - d_2)\, z^{-1}}, \tag{3}$$

where $d_1 = \exp(-Ts/M)$, $d_2 = \exp(-Ts/m)$ and Ts is the sampling rate period (corresponding to the ADC sampling rate). Then equation (3) can be rewritten as

$$(d_1 - d_2)\, z^{-1}\, V_o[z] = \left(1 - d_1 z^{-1}\right)\left(1 - d_2 z^{-1}\right) V_i[z]. \tag{4}$$

After inverse Z transformation, the recursive model in the time domain can be obtained,

$$v_o[n-1] = \frac{v_i[n] - (d_1 + d_2)\, v_i[n-1] + d_1 d_2 v_i[n-2]}{(d_1 - d_2)}. \tag{5}$$

According to equation (1), pile-up pulses are simulated with $M = 50Ts$ and $m = 2.5Ts$. The simulated dual-exponential pulses are illustrated in Fig. 2. Equation (5) is used to obtain

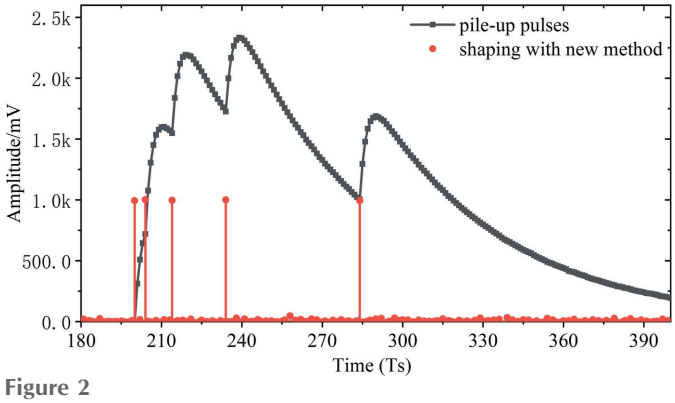

Figure 2
Simulation of dual-exponential pulse pile-up discrimination.

the output signal of the discrimination system. It can be seen that the proposed method can identify the pile-up pulse.

According to the decomposition principle of a cascade system, equation (3) can be written as a cascade equation, *i.e.*

$$H(z) = H_1(z)\, H_2(z)\, H_3(z)\, H_4(z), \tag{6}$$

where

$$H_1(z) = (1 - d_1 z^{-1}), \qquad H_2(z) = (1 - d_2 z^{-1}),$$
$$H_3(z) = z, \qquad H_4(z) = \frac{1}{d_1 + d_2}.$$

Module H_1 can shorten the slow component of the dual-exponential and H_2 can reduce the fast component of the dual-exponential. H_3 is a leading bit system, used to align the moment of pulses generation; H_4 is an amplification system. The impulse pulse is finally obtained after one clock delay. Equations (7), (8), (9) and (10) can be obtained from the inverse transformation of equation (6),

$$v_1(n) = v_i(n) - d_1 v_i(n-1), \tag{7}$$

$$v_2(n) = v_1(n) - d_2 v_1(n-1), \tag{8}$$

$$v_3(n) = v_2(n+1), \tag{9}$$

$$v_o(n) = \frac{v_3(n)}{(d_1 - d_2)}. \tag{10}$$

2.2. Selection of the shaping parameters

2.2.1. Module H_1. In the system, module H_1 shapes the slow component of the dual-exponential pulse into an impulse signal to reduce the system dead-time. In Fig. 3(*a*), a dual-exponential pulse is acquired and converted with a high-performance silicon drift detector (fast SDD) and ADC [20 Megasamples per second (MSPS)]. According to the fitting calculation, the decay constants of the slow and fast component are $M \simeq 2.5$ µs and $m \simeq 83$ ns, respectively. Therefore, the theoretical values of the parameters d_1 and d_2 in equation (5) are $d_1^* = \exp(-1/50)$ and $d_2^* = \exp(-3/5)$. Letting $d_1 = \exp(-1/10)$, $\exp(-1/50)$ and $\exp(-1/200)$, respectively, according to equation (7), the output signals of the intermediate system v_1 are displayed in Figs. 3(*b*), 3(*c*) and 3(*d*).

It can be seen that there still exists tailing in v_1 when $d_1 < d_1^*$, and v_1 becomes a bipolar signal when $d_1 > d_1^*$. The long tailing due to the slow component of the dual-exponential pulse can be reduced as $d_1 = d_1^*$.

2.2.2. Module H_2. Module H_2 shapes the fast component of the dual-exponential pulse into an impulse signal to reduce the dead-time. H_3 is only a delay to H_2. H_4 is an amplification module; the performance of the module H_2 can be obtained by analyzing the output v_o. In order to obtain an optimal d_2, the output of the impulse pulse-shaping system v_o should be simulated and discussed. Under the condition $d_1 = d_1^*$, different parameters of d_2 are simulated to test the performance of peak pile-up identification. The simulation results are illustrated in Figs. 4(*b*), 4(*c*) and 4(*d*).

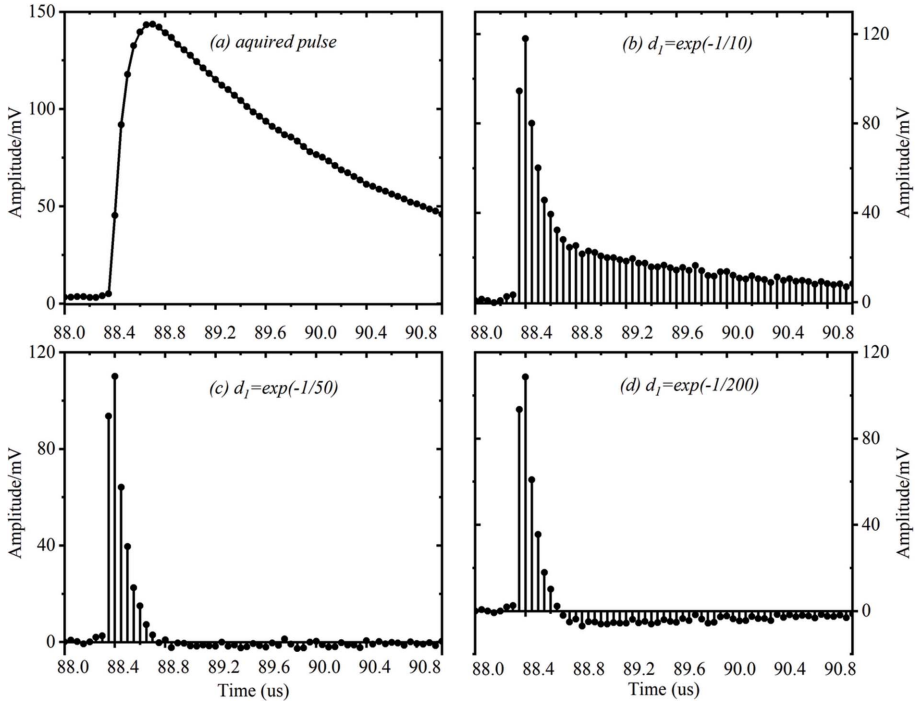

Figure 3
Relationship between system output and parameter d_1 and d_1^*.

Fig. 4(*b*) indicates that there is a reverse impulse sequence in v_o when $d_2 > d_2^*$; and the reverse component can be reduced if $d_2 = d_2^*$.

Although the output is a synthetic polar impulse sequence when $d_2 < d_2^*$, the width of the shaped pulse is 250 ns.

The output in Fig. 4(*c*) is the response of the system with $d_2 = d_2^*$ and the pulse width is 100 ns instead of the theoretical 50 ns. This is because the real nuclear signal is not a strictly dual-exponential signal but only a dual-exponential-like pulse signal.

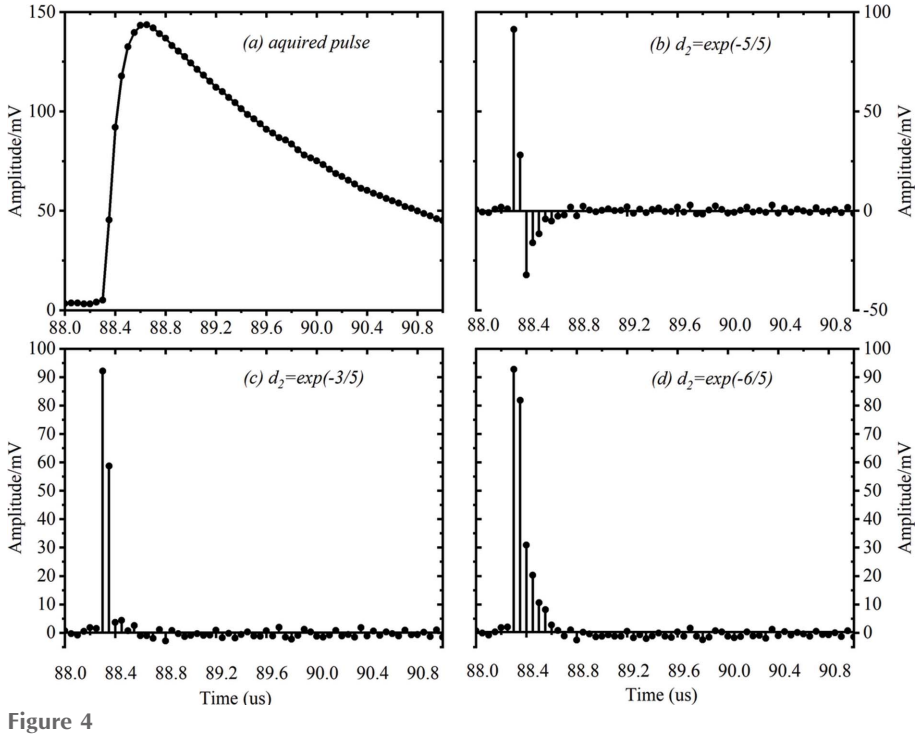

Figure 4
Relationship between system output and parameter d_2 when $d_1 = d_1$*.

3. Counting loss correction in the fast channel

The distribution of the intervals between random events is

$$p(t) = \lambda \exp(-\lambda t), \tag{11}$$

where λ is the exponential distribution constant, representing the average pulse counting rate. When the interval time of two consecutive pulses is less than the dead-time $t_{\rm pileup}$, the fast-shaping method cannot discriminate, and the two pulses will be misidentified as one pulse and result in a loss of counting rate. When the interval time of two consecutive pulses is longer than the dead-time $t_{\rm pileup}$, the pulse is recorded, and the probability of the measured pulse is given by

$$p\left(t_1 > t_{\rm pileup}\right) = \exp\left(-\lambda t_{\rm pileup}\right). \tag{12}$$

Therefore, the correction formula between the real pulse counting rate $R_{\rm real}$ and the measured pulse counting rate $R_{\rm measure}$ is

$$R_{\rm real} \exp\left(-\lambda t_{\rm pileup}\right) = R_{\rm measure}. \tag{13}$$

Equation (13) is an implicit equation and has two solutions. The slow channel cannot directly perform self-correction, and it needs to be corrected assisted by the fast channel. In the fast channel, when the counting loss is not severe, equation (13) can be used to perform the counting rate correction, and the smaller value of the two solutions should be taken as the result of the counting rate correction.

4. Experiment

4.1. Experimental conditions and comparative analysis

A data acquiring board embedded with a 20 MSPS 14-bit ADC was developed by Sichuan X-STAR Technology (M&C Co. Ltd). An Amptek fast-SDD detector was used to acquire the pulse signal; it has a 25 mm^2 active area, a thickness of 500 µm and a 0.5 mil Be window. Dual-exponential-like pulse

sequences with a less than 300 ns rising edge and decay constant of 3.2 µs were acquired. Some experimental pulses based on an XRF platform were also obtained from the Sichuan X-STAR.

An X-ray tube with Ag target was used to irradiate an MnO_2 sample; the tube voltage was set to 33.3 kV while the tube current varied from 3.9 µA to 160.8 µA. A vacuum pump was used to evacuate; the vacuum degree was about 0.093 MPa.

Fig. 5(*a*) shows a section of original pulses data acquired at 160.8 µA. The single-exponential impulse fast-shaping method (Huang *et al.*, 2017; Hong *et al.*, 2018) was used to shape the acquired pulses, as shown in Fig. 5(*b*). The tailing of the fast-shaping output narrow-beam signal has an exponential attenuation characteristic, so the single-exponential impulse shaping only eliminates the slow component of the dual-exponential pulse while the fast component still exists. The time width of the fast component output signal in Fig. 5(*b*) is approximately 300 ns; it is close to the rise time of the acquired pulse. Fig. 5(*c*) shows the processing result of the collected pulses data using the dual-exponential impulse shaping method proposed in this paper, and the output is a narrow impulse signal of which the width is about 100–150 ns.

4.2. Results analysis

The calculation results of the counting rate under different currents is shown in Table 1. The dual-exponential impulse shaping method with parameters $d_1 = \exp(-1/50)$ and $d_2 = \exp(-3/5)$ is used for pulse shaping. R_{f1} and R_{f2} represent the counting rate obtained with the dual-exponential impulse shaping method and the single exponential impulse shaping method, respectively.

R_{f1c} and R_{f2c} are the corrected results of R_{f1} and R_{f2}, respectively, and the dead-time $t_{\text{pile-up}}$ of the dual-exponential impulse shaping is 150 ns while that of the single-exponential impulse shaping is 300 ns.

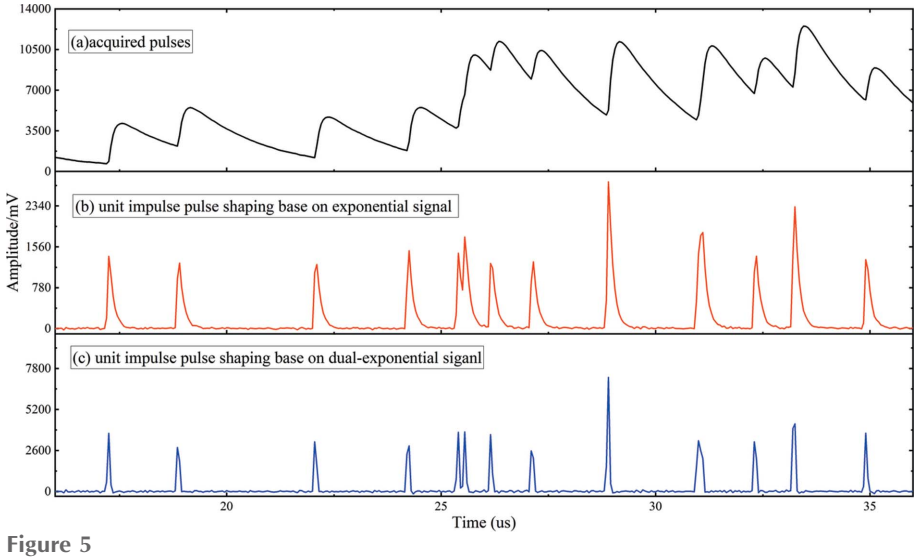

Figure 5
Comparison of dual-exponential and single exponential rapid shaping.

Table 1
Test results and error analysis of the dual-exponential impulse shaping counting rate and single exponential fast shaping counting rate.

Current (µA)	R_{f1} (cps)	R_{f2} (cps)	R_{cal} (cps)	$(R_{f1} - R_{cal})/R_{cal} \times 100$	$(R_{f2} - R_{cal})/R_{cal} \times 100$
3.9	18113.6	18039.84	18113.6	–	–
7.8	35667.6	35392.48	36227.2	−1.54	−2.30
19.6	87299.04	85750.72	91032.45	−4.10	−5.80
31.4	137694.64	133803.44	145837.70	−5.58	−8.25
43.1	187122.48	179955.12	200178.50	−6.52	−10.10
54.9	235764.24	224313.04	254983.75	−7.53	−12.02
66.7	283972.48	267369.52	309789.00	−8.33	−13.69
78.4	330456.64	307879.2	364129.80	−9.247	−15.44
90.2	375808.64	346500.48	418935.05	−10.29	−17.29
102	419772.56	383127.84	473740.30	−11.39	−19.12
113.7	462556.8	417992.48	528081.10	−12.40	−20.84
125.5	504771.68	451667.12	582886.3	−13.40	−22.51
137.3	546055.36	483875.92	637691.61	−14.36	−24.12
149	584720.08	513246.08	6920320.41	−15.50	−25.83
160.8	622314.72	541458.48	746837.66	−16.67	−27.49

When the X-ray tube current is 3.9 µA, the counting rate is relatively low, then $R_f = R_{real}$. When the other experiment variables are the same, the amount of emitted beam from the X-ray tube is proportional to the tube current; then the true counting rate R_{cal} is derived from the counting rate R_f measured at the current of 3.9 µA,

$$R_{cal} = kI, \tag{14}$$

where k is a constant; when the current is weak, $k = R_f/I$ and I represents the X-ray tube current.

Fig. 6 shows the relationship between counting rate and current. As the current increases, the counting rate increases. Also, as the X-ray tube current increases, the pile-up pulse increases.

It can be seen from Fig. 6 that the counting rate of dual-exponential impulse shaping is higher than that of single exponential impulse shaping. After the counting rate correction, the counting rate of dual-exponential impulse shaping is closer to the real value. Table 1 shows R_{f1}, R_{f2} and their errors relative to R_{cal}, and Table 2 shows R_{f1c}, R_{f2c} and their relative errors with R_{cal} as the tube current increases.

The relative errors of R_{f1} and R_{f2} gradually increase as the tube current increases. When the current is maximum at 160.8 µA, the pulse incidence rate is 746 kcps theoretically. The pulses counting rate identified with the dual-exponential impulse shaping method is 622 kcps, and the relative error is −16.67%. The pulse counting rate identified with single exponential impulse fast shaping is 541 kcps, and the relative error is −27.49%. The results using the dead-time correction are shown in Table 2.

After dead-time correction, the counting rate acquired using dual-exponential impulse shaping is 690 kcps

Table 2
Counting statistics and error analysis after correction.

Current (μA)	R_{f1c} (cps)	R_{f2c} (cps)	R_{cal}	$(R_{f1c} - R_{cal})/R_{cal} \times 100$	$(R_{f2c} - R_{cal})/R_{cal} \times 100$
3.9	18167.94	18148.07	18113.6	–	–
7.8	35845.93	35764.1	36227.2	−1.05	−1.27
19.6	88433.92	88065.98	91032.45	−2.85	−3.25
31.4	140586.22	139423.18	145837.70	−3.60	−4.39
43.1	192549.03	190482.49	200178.50	−3.81	−4.84
54.9	244487.51	241136.51	254983.75	−4.11	−5.43
66.7	297035.21	291833.83	309789.00	−4.11	−5.79
78.4	348301.29	341130.15	364129.80	−4.35	−6.31
90.2	399108.77	389639.78	418935.05	−4.73	−6.99
102	449156.63	436574.17	473740.30	−5.18	−7.84
113.7	498636.23	483199.30	528081.10	−5.57	−8.49
125.5	548182.04	529579.69	582886.35	−5.95	−9.14
137.3	597384.56	575328.46	637691.61	−6.32	−9.77
149	643776.80	617948.28	6920320.41	−6.97	−10.70
160.8	690147.02	660037.88	746837.66	−7.59	−11.62

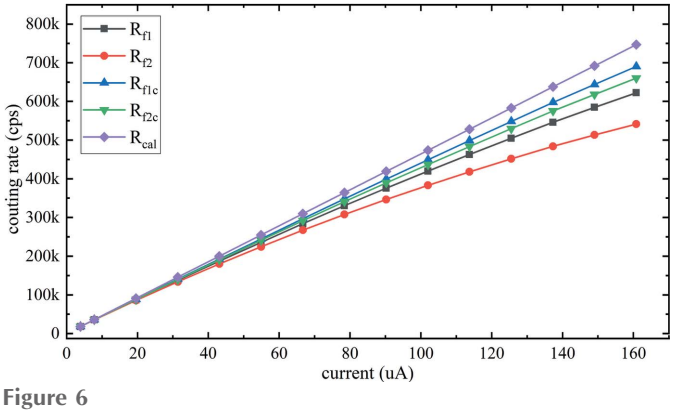

Figure 6
The counting rate as a function of the current.

with a relative error of −7.9%, while that acquired using the single exponential impulse fast-shaping method is 660 kcps with a relative error of −11.62%. Therefore, the dual-exponential impulse shaping algorithm has a better pulse recognition ability.

5. Conclusion

This paper proposed a new dual-exponential impulse shaping method for pulse shaping in the fast channel. The output signal of the fast SDD is a dual-exponential-like pulse signal with a fast and slow component. The application of the new method can not only eliminate the long tailing of the slow component but also weaken the tailing of the fast component. A comparison between the new method and the single exponential impulse fast-shaping method is made. The output pulse width of the fast channel with the new method is about 100–150 ns, while for the single exponential impulse fast-shaping method it is approximately 300 ns; the dead-time of the pulse identification can be reduced significantly with the new method. Different X-ray tube currents are set: Mn in the high purity sample MnO_2 is measured for 100 s with the fast SDD, as the current is maximum at 160.8 μA and the counting rate loss is most severe. Before the counting rate correction, the relative error with regard to the real counting rate is −16.67% with the new method, while for the single exponential impulse fast-shaping method it is −27.49%; after the counting rate loss correction, the relative error with regard to the real counting rate is −7.9% with the new method, while for the single exponential impulse fast-shaping method it is −11.62%. Thus, the counting rate obtained by the proposed dual-exponential impulse pulse-shaping method is closer to the real counting rate. As mentioned in the discussion above, the new method proposed in this paper can not only shorten the dead-time but also can be used to effectively correct the counting rate under the condition of a high counting rate.

Funding information

The following funding is acknowledged: National Natural Science Foundation of China (grant No. 11975060); Major science and technology projects of Sichuan Province (grant No. 19ZDZX).

References

Bolić, M. & Drndarević, V. (2002). *Nucl. Instrum. Methods Phys. Res. A*, **482**, 761–766.
Cano-Ott, D., Tain, J. L., Gadea, A., Rubio, B., Batist, L., Karny, M. & Roeckl, E. (1999). *Nucl. Instrum. Methods Phys. Res. A*, **430**, 488–497.
Ehrenberg, J. E., Ewart, T. E. & Morris, R. D. (1978). *J. Acoust. Soc. Am.* **63**, 1861–1865.
Hong, X., Zhou, J., Ni, S., Ma, Y., Yao, J., Zhou, W., Liu, Y. & Wang, M. (2018). *J. Synchrotron Rad.* **25**, 505–513.
Huang, Y., Gong, H. & Li, J. (2017). *J. Tsinghua Univ. (Sci. Technol.)*, **57**, 512–524.
Imperiale, C. & Imperiale, A. (2001). *Measurement*, **30**, 49–73.
Jordanov, V. T. (2016). *Nucl. Instrum. Methods Phys. Res. A*, **805**, 63–71.
Jordanov, V. T. & Knoll, G. F. (1994). *Nucl. Instrum. Methods Phys. Res. A*, **345**, 337–345.
Sun, C., Rao, K.-Y., Guo, J.-F., Zhang, H.-B., Dong, Y.-J. & Wu, J.-P. (2017). *Nucl. Electron. Detect. Technol.* **37**, 752–756.